Archives of Biochemistry and Biophysics 774 (2025) 110628

Contents lists available at ScienceDirect

Archives of Biochemistry and Biophysics

journal homepage: www.elsevier.com/locate/yabbi

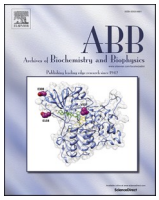

"Single molecule tracking unveils distinct FcγRIIB and FcRn plasma membrane dynamics"

Marta Rojas-Rodríguez [a], Francesco Saverio Pavone [a,b], Martino Calamai [a,c,*]

[a] European Laboratory for Non-linear Spectroscopy, Via Nello Carrara 1, 50019, Sesto Fiorentino, Italy
[b] Department of Physics and Astronomy, University of Florence, Via G. Sansone 1, 50019, Sesto Fiorentino, Italy
[c] National Institute of Optics –National Research Council (CNR-INO), 50019, Sesto Fiorentino, Italy

ARTICLE INFO

Keywords:
Fc receptors
Cellular distribution
Single molecule
Diffusion
Trafficking

ABSTRACT

Fc receptors (FcRs) constitute a heterogeneous family of membrane-bound proteins that are integral to the immune system function, primarily through their ability to bind the constant domain (Fc) of antibodies. These receptors mediate a variety of immunological processes and maintain immunological homeostasis. FcRs exhibit a broad distribution throughout the body, being expressed not only on the surface of various immune cells but also in non-immune cells and tissues. Over the past decade, specific FcRs -most notably the neonatal Fc receptor (FcRn) and Fc gamma receptor IIb (FcγRIIB)- have emerged as putative mediators in processes such as antibody-mediated uptake. However, the literature presents conflicting evidence regarding their precise roles and mechanisms in antibody internalization. In this study, we employed single molecule tracking in living epithelial-like cells to investigate the cellular distribution and dynamics of FcγRIIB and FcRn, basic features that are still largely uncharacterized. Our findings revealed that FcγRIIB, mostly present on the cell membrane, is highly mobile and can be actively internalized. Conversely, FcRn was primarily localized intracellularly, with only a minor fraction capable of reaching the cell surface, where it exhibited minimal mobility. These results show that FcγRIIB, but not FcRn, displays the basic expected requisites that would be necessary for surface antibody binding and uptake.

1. Introduction

Fc receptors (FcRs) are specialized proteins with high binding specificity for the constant Fc domain of antibodies. These receptors are classified based on the antibody isotype that they recognize, their role in regulating immune responses to infections, and their function in controlling inflammation processes [1].

Fc gamma receptor IIb (FcγRIIB) is a type I transmembrane protein characterized by a single-pass helical transmembrane domain and a cytoplasmic tail containing an immunoreceptor tyrosine-based inhibition motif (ITIM) [2]. FcγRIIB (encoded by the FCGR2B gene) exists in two main isoforms—FcγRIIB1 and FcγRIIB2—generated through alternative splicing of the FCGR2B mRNA [3]. Although FcγRIIB1 and FcγRIIB2 share similar signaling pathways, their primary functional distinction lies in their subcellular localization and internalization behavior. FcγRIIB1 contains a unique 19-amino acid C1 insertion in its cytoplasmic tail, which anchors it more stably at the plasma membrane, thereby limiting its internalization. In contrast, FcγRIIB2 lacks this insertion and is rapidly endocytosed upon ligand binding [4,5]. Uniquely among Fc gamma receptors, FcγRIIB functions as an inhibitory receptor, playing a crucial role in downregulating immune responses and preventing excessive inflammation and autoimmunity. It also contributes to immune homeostasis through the clearance of immune complexes [5,6]. FcγRIIB is predominantly expressed on B cells, monocytes, macrophages, and dendritic cells [5]. According to the Human Protein Atlas, it exhibits high expression in the placenta and medium expression in the respiratory system. Expression has also been reported in non-immune tissues, including the liver [7], gastrointestinal tract mast cells [8], human airway smooth muscle cells [9], and placental endothelial cells [10]. Notably, emerging studies suggest an additional role for FcγRIIB in mediating IgG transport and trafficking across epithelial barriers in various tissues [11–13], including targeting IgGs to lysosomal degradation pathways [9]. However, the precise mechanisms regulating these processes remain to be fully elucidated.

An additional Fc receptor, the neonatal Fc receptor (FcRn), has emerged as putative candidate for the uptake and intracellular transport

* Corresponding author. National Institute of Optics – National Research Council (CNR-INO), via Nello Carrara 1, 50019, Sesto Fiorentino, Italy.
E-mail address: martino.calamai@cnr.it (M. Calamai).

https://doi.org/10.1016/j.abb.2025.110628
Received 21 March 2025; Received in revised form 28 August 2025; Accepted 25 September 2025
Available online 26 September 2025

of IgGs as a consequence to its originally discovered role of transferring IgGs from the mother to the fetus across the placenta through a polarized cell layer [14]. FcRn is associated with β-2-microglobulin (β2M), forming a heterodimer with a structure similar to the major histocompatibility complex (MHC) class I. This receptor is primarily involved in regulating the half-life of IgGs and albumin by protecting them from lysosomal degradation [15]. Although the expression pattern in humans is not yet fully known, this receptor has been found in tissues other than the placenta, such as different types of epithelia in the intestine [16,17], kidney [18] and liver [19]. FcRn is also expressed in the microvascular endothelium cells of the BBB [20], but the precise localization in the vascular endothelium is yet to be defined [21]. The role of this receptor in other tissues remains unclear. While FcRn plays a known role in IgG directional transport across polarized epithelial cells [22] and might be associated with efflux transport in the endothelial cells of the BBB [20], some authors claim that FcRn has an important role in IgG clearance from the brain [23], whereas for others it participates only marginally to the IgG transport across brain endothelial cells [24], or in the overall brain distribution of IgGs [25,26]. Recent findings in murine models indicate that neither FcRn, nor FcγRIIB [25], seem to contribute significantly to IgG binding and intracellular trafficking. Nonetheless, FcγRIIB has been shown to play a role in maternal IgG transport across human placental endothelial cells [27], although other studies have proposed that it is FcRn, rather than Fcγ receptors, that mediates this process in the placenta [28]. Additionally, FcγRII expression has been detected in the olfactory epithelium [13], raising the possibility that FcγRs could participate in IgG trafficking at other barrier interfaces such as the airway.

In this study, we focused on precisely characterizing the cellular localization and plasma membrane dynamics of FcγRIIB (isoform 1) and FcRn receptors in living epithelial cells by means of genetically engineered chimeric constructs and single molecule tracking, an important essential, but rather understated, information to properly evaluate the role of these two receptors in IgG binding, internalization and trafficking.

2. Materials and methods

2.1. Cloning

To generate the fusion constructs AP-FcRn-mBFP and AP-FCGR2B-mBFP, two different plasmids were used with the sequences contained in the vector pCMV6-ENTRY (NM_001136019 for FcRn and NM_004001 for FCGR2B transcript variant 1, Origene).

To develop the *AP-FcRn-mBFP* plasmid, first, two new restriction sites (*Nhe*I, *Asc*I) were added right after the signal peptide (SP) using the QuikChange Lightning Site-Directed Mutagenesis Kit (Agilent Technologies) with 5′-GAGCCTGGGCGCAGCTAGCCAGGGCGCGCCAGAAAGC CACCTCTC-3′ as a forward primer and 5′-GAGAGGTGGCTTTCTG GCGCGCCCTGGCTAGCTGCGCCCAGGCTCC-3′ as a reverse primer. Then, the genetic AP tag was added by inserting the annealed oligos after opening the plasmid with *Nhe*I and *Asc*I (forward oligo: 5′-CTAGCGAGGGCCTGAACGATATCTTCGAGGCCCAGAAGATCGAGT GGCACGAGAGTGG-3′ reverse oligo: 5′-CGCGCCACTCTCGTGCCACTC-GATCTTCTGGGCCTCGAAGATATCGTTCAGGCCCTCG-3′). After adding the AP tag, a monomeric variant blue fluorescent protein (mBFP) [29] in the C-terminal part of the FcRn was added. mBFP was extracted from the plasmid Adam10-mBFP [30] by PCR reaction (Forward primer 5′-TAAGCAACGCGTATGAGCGAGCTGATTAAGGA-3′, reverse primer 5′-TGGGGCACAAGCTTAATTAACTCGAGTAAGCA-3′). Subsequently, the sequence of the mBFP was inserted after opening the FcRn plasmid with *Mlu*I and *Xho*I, obtaining the final product *AP-FcRn-mBFP*.

To develop the *AP-FCGR2B-mBFP* plasmid the same strategy was followed. Two new restriction sites (*Nhe*I, *Asc*I) were added right after the SP using the QuikChange Lightning Site-Directed Mutagenesis Kit (Agilent Technologies) with 5′-CTCCTGTTGCTGGGGCTAGCCAGGG CGCGCCAACACCTGCAGCTCC-3′ as a forward primer and 5′-GGAGCTGCAGGTGTTGGCGCGCCCTGGCTAGCCCCAGCAACAGGAG-3′ as a reverse. Then, the AP tag was added by inserting the annealed oligos after opening the plasmid with *Nhe*I and *Asc*I (forward and reverse oligos: 5′-CTAGCGAGGGCCTGAACGATATCTTCGAGGCCCAGAAGATC GAGTGGCACGAGAGTGG-3′, 5′-CGCGCCACTCTCGTGCCACTCGATCT TCTGGGCCTCGAAGATATCGTTCAGGCCCTCG-3′). After adding the AP tag, a mBFP in the C-terminal part of the FCGR2B was included. The fluorescent protein mBFP was extracted from the plasmid AP-Bace1-mBFP (previously developed in our lab) by a restriction reaction with *Mlu*I and SacII and gel extraction. Then inserted in the AP-FCGR2B plasmid previously open with the same enzymes (*Mlu*I, SacII), obtaining the final product *AP-FCGR2B-mBFP*.

To develop the *mCherry-β2M* plasmid the fluorescent protein mCherry was extracted from the plasmid pmCherry-N1 (plasmid Cat. No. 632523, Clontech) by PCR reaction (Forward primer 5′- TAAG-CAacgcgtATGGTGAGCAAGGGCGAGGA-3′, reverse primer 5′-TGCTTActcgagCTACTTGTACAGCTCGTCCATGC-3′) in order to add the *Mlu*I and *Xho*I restriction sites. Then inserted in the β2-microglobulin (β2M) plasmid (NM_004048, Origene) previously open with the same enzymes (*Mlu*I, *Xho*I), obtaining the final product *mCherry-β2M*.

2.2. Cell cultures

T24 (Bladder carcinoma, epithelial like) and HEK293t (Human embryonic kidney) cells from American Type Culture Collection (A.T.C.C.) were cultured in Dulbecco's Modified Eagle Medium (DMEM), (ThermoFisher Scientific) supplemented with 1 % penicillin/streptomycin solution and 10 % fetal bovine serum (FBS). Cell cultures were incubated at 37 °C, 5 % CO_2 in a humidified atmosphere. Cell cultures were grown to 90 % confluency.

T24 bladder epithelial cells and HEK293t cells were used in this study. Both are highly transfectable and widely employed for studies on membrane receptor dynamics and trafficking. T24 cells were chosen as the primary model, as they retain key epithelial characteristics relevant for analyzing receptor behavior at the cell surface, while HEK293t cells served as a secondary system to validate observations.

2.3. Cell transfection

T24 and HEK293t cells were plated on 18 mm glass coverslips in 12-well plates at 100000 cells per well. 24 h after plating HEK293t cells were transfected with Lipofectamine 2000 (ThermoFisher Scientific) according to the manufacturer's instructions, with 1 μg DNA in total and 2 μL Lipofectamine in OPTIMEM medium (ThermoFisher Scientific), 24 or 48 h before imaging. T24 cells were transfected with FuGene HD (Promega) according to the manufacturer's instructions, with 1 μg DNA in total and 3 μL FuGene in OPTIMEM medium, 24–48 h before imaging.

For experiments with *AP-FcRn-mBFP*, cells were co-transfected with β2M using a commercially available, validated construct widely used in published studies (NM_004048, Origene) and Bir A [31], a biotin ligase that specifically binds biotin to the AP tag. Biotin is added to the cell media at 10 mM final concentration, 8 h after transfection and 12 h before imaging or flow cytometry analysis [32].

For experiments with *AP-FCGR2B-mBFP*, cells were co-transfected with Bir A.

2.4. Cell labeling for imaging

For labeling, 24–48h after transfection, cells were fixed for 10 min at

room temperature (RT) with 4 % (w/v) paraformaldehyde (PFA), washed with phosphate buffer saline (PBS) (supplemented with CMgCl2 0,5 mM, CCaCl2 0,8 mM) and permeabilized for 10 min at RT with 0.075 % Triton X. The samples only fixed and not permeabilized for surface labeling skipped the permeabilization step.

After washing with PBS, cells were blocked for 30–60 min with 4 % bovine serum albumin (BSA) in PBS. Cells were labeled with different combinations of fluorophores and antibodies and all of them were diluted in PBS with 4 % BSA.

For Figs. 1b, 3b and 4c, Alexa Fluor™ 488 conjugated with streptavidin for 30 min at RT (1:1000 ThermoFisher Scientific).

For Figs. 1c and 3c, Alexa Fluor™ 488 conjugated with streptavidin for 30 min at RT (1:1000 ThermoFisher Scientific) and wheat germ agglutinin (WGA) Alexa Fluor™ 594 for 30 min at RT (1:500 ThermoFisher Scientific).

For Fig. S1 and S2, primary anti-FcRn 488 for 60 min at RT (1:250 mouse anti-human, sc-271745 AF488, Santa Cruz).

For Fig. S3, primary anti-FcRn for 40 min at RT (1:250 rabbit anti-FcRn PA5-97738, ThermoFisher Scientific), secondary antibody for 30 min at RT (1:500 donkey anti-rabbit AlexaFluor 568, ThermoFisher Scientific) and Alexa Fluor™ 488 conjugated with streptavidin for 30 min at RT (1:1000 ThermoFisher Scientific).

2.5. Confocal microscopy analysis

The analysis was performed with a Nikon Eclipse TE300C2 LCSM (Nikon) equipped with a Nikon Plan Apo 60x 1.4 NA immersion oil immersion objective or Plan Apo λ 100x 1.49 NA oil immersion objective and with Coherent CUBE (diode 405 nm), Melles Griot (Argon 488 nm) and Coherent Sapphire (Sapphire 561 nm) lasers. Emission filters for imaging were 452/45 nm, 514/30 nm and 595/60 nm. For each sample, optical sections at median planes of the cells were taken (1024x1024 pixels) using sub-saturation settings and all of them were kept constant for each analysis (laser power, detector gain, and pinhole diameter). Images were processed and analyzed with the Fiji software and Origin (Pro) ("Version 2022b", OriginLab Corporation).

2.6. Intracellular colocalization with subcellular compartments

For the intracellular colocalization with organelles experiments, cells were co-transfected with AP-FcRn-mBFP or AP-FCGR2B-mBFP and the plasmid for the specific subcellular compartment.

For Golgi apparatus mEmerald-TGNP-N-10 (Addgene, plasmid #54279), for endoplasmic reticulum mEmerald-Calnexin-N-14 (Addgene, plasmid #54021), for early endosomes, GFP-EEA1wt (Addgene, plasmid #42307) [33].

For lysosomes staining, cells were incubated with LysoTracker™ Red DND-99 (ThermoFisher Scientific) at a final concentration of 1uM for 30 min at 37 °C.

For plasma membrane staining, cells were incubated with WGA Alexa Fluor™ 594 for 30 min at 37 °C (1:500, ThermoFisher Scientific).

For live cell imaging, living T24 cells 24 h after transfection were washed with PBS one time and the media was replaced with Leibovitz's L-15 (ThermoFisher Scientific) supplemented with 2 % FBS.

The analysis was performed as explained in the previous section (confocal microscopy analysis) using 488 nm excitation for Golgi apparatus, endoplasmic reticulum and early endosomes and 561 nm excitation for lysosomes and plasma membrane.

To characterize the colocalization degree between the subcellular compartment and the receptors, the JACoP plugin [34] for Fiji software was used. Specifically, to calculate Pearson's correlation coefficient [35], which estimates the covariance of signal intensities between two images by analyzing them on a pixel-by-pixel basis, and Manders' overlap coefficient [36], which measures the fraction of pixels in image 1 that overlap with those in image 2, and vice versa. The data was analyzed with Origin (Pro).

2.7. Flow cytometry analysis

T24 cells co-transfected with AP-FcRn-mBFP, Bir A and β2M or AP-FCGR2B-mBFP and BirA were washed with PBS and harvested in DMEM after mild trypsin treatment 24 h after transfection. A BD Cytofix/CytopermTM Fixation/Permeabilization Solution kit (BD Biosciences, Lake Franklin, NJ, USA) was used for fixation and permeabilization according to the manufacturer's instructions.

For experiments with AP-FcRn-mBFP, Bir A and β2M, cells were incubated with anti-β2M primary antibody for 60 min at RT (1:100, rabbit anti β2M (D8P1H) Cell signaling technology) followed by a secondary antibody for 30 min at RT (1:1000 mouse anti-rabbit AlexaFluor 647, ThermoFisher Scientific) and Alexa Fluor™ 488 conjugated with streptavidin for 30 min at RT (1:1000 ThermoFisher Scientific).

For experiments with AP-FCGR2B-mBFP and BirA cells were incubated with Alexa Fluor™ 488 conjugated with streptavidin for 30 min at RT (1:1000 ThermoFisher Scientific).

All the fluorophores and antibodies were diluted in 1 × BD Perm/Wash buffer. After 3x washing with 1 × BD Perm/Wash buffer samples were analyzed using the Accuri-C6 flow cytometer (BD Biosciences, Lake Franklin, NJ, USA) equipped with 488 nm and 640 nm lasers. Green-fluorescence was excited using the 488 nm laser, and the emitted fluorescence was collected through a 530/15 nm band-pass filter. Red fluorescence was excited using the 640 nm laser and the emitted fluorescence was collected through a 675/12.5 nm band-pass filter. Data was analyzed using the BD Accuri-C6 software. The cellular debris was excluded by gating cells on the Forward scatter area/Side scatter area (FSC/SSC). Approximately 25000 events were acquired for each sample.

2.8. Single molecule imaging and tracking

The methodologies for quantum dots (QDs) surface labeling and live imaging used in this study, have been already reported [37–39].

Living T24 cells transfected for 24–48 h with the AP-FcRn-mBFP, Bir A and β2M, or AP-FCGR2B-mBFP and Bir A plasmids, were incubated in Leibovitz's L-15 medium 2 % FBS at 37 °C with Qdot™ 655 streptavidin conjugate (1:10.000 Invitrogen) in QD binding buffer [37] for 5–10 min, and washed afterwards.

Cells were analyzed with an Olympus IX2-UCB wide-field epifluorescence microscope equipped with a 100× UPlanSAPO Olympus oil-immersion objective, a four-channel LED Driver Thorlabs DC4014 (using 405 excitation LED) and a custom heating chamber. Dichoric FF552-Di02 and emission FF02-655/40-25 filters were used for QDs emitting at 655 nm. All filters were from Semrock. Single-molecule tracking was performed at 37 °C with recordings of 30 s per cell, at a temporal resolution of 1 frame every 100 ms. This acquisition speed allows for reliable detection of receptor mobility at the plasma membrane. Movies were acquired with an Electron Multiplying Charge-Coupled Image MX2 camera (Hamamatsu). Recording sessions did not last more than 30 min. Tracking and analysis of single QDs reconstructing the trajectories was performed with TrackMate [40]. Only trajectories with a minimum of 30 consecutive steps were further analyzed. Then with the selected trajectories, the mean squared displacement (MSD) of the trajectories was calculated with TraJClassifier [41]. The MSD measurements can be compared with simulation models to identify the trafficking dynamics of the receptor [41]. This Fiji plugin loads the trajectories from TrackMate, identifies and classifies

them into normal diffusion, subdiffusion, confined diffusion and directed/active motion by a random forest approach. Moreover, other parameters such as the diffusion coefficient (D), mean velocity, exponent α as well as confidence values, MSD ratio and fractal dimension are automatically calculated [41], providing a very detailed and robust characterization of the trajectories.

3. Results

3.1. Cellular localization of FcγRIIB

We genetically engineered a versatile FcγRIIB construct (AP-FCGR2B-mBFP) that bears the short biotin acceptor peptide tag (AP) [31] at the N-terminus, immediately after the signal peptide (SP), and a monomeric blue fluorescent protein (mBFP) [29] at the C-terminus. The construct was co-transfected in T24 cells with a plasmid encoding for the ER targeted BirA [31,32], which specifically biotinylates the AP tag.

To ensure that the genetically engineered AP-FCGR2B-mBFP construct was correctly expressed and that the biotinylated AP tag was accessible for further labeling, transfected T24 cells were fixed, permeabilized and labeled with streptavidin conjugated with Alexa Fluor™ 488, which binds specifically to the biotinylated AP tag (Fig. 1a and b). The resulting co-localization of mBFP and streptavidin Alexa Fluor™ 488 support the proper expression of AP-FCGR2B-mBFP. Proper high expression levels of AP-FCGR2B-mBFP were also tested with flow cytometry (Fig. S4).

On the other hand, to exclusively assess the presence of AP-FCGR2B-mBFP on the cell surface, transfected cells were only fixed (not permeabilized) and subsequently labeled with streptavidin Alexa Fluor™ 488 and with WGA Alexa Fluor™ 594, a commonly used marker that binds specifically to the sialic acid present in the plasma membrane [42] (Fig. 1c). The co-localization of the three fluorescent markers demonstrates that AP-FCGR2B-mBFP is efficiently targeted to the cell membrane.

In order to further characterize the cellular distribution of the receptor within T24 cells, we quantified the potential co-localization between AP-FCGR2B-mBFP and the markers of the Golgi apparatus, endoplasmic reticulum, early endosomes, lysosomes and plasma membrane (Fig. 2a–c). As expected, the plasma membrane showed the highest level of co-localization, as demonstrated by the calculated Pearson's (0.74 ± 0.01) and M1/M2 Mander's coefficients (M1 = 0.76 ± 0.03; M2 = 0.78 ± 0.02, with M1 referring to the degree of overlap of FcγRIIB with the plasma membrane marker, and M2 referring to the inverse overlap). The co-localization with the Golgi apparatus was more modest, with a Pearson's coefficient of 0.52 ± 0.02, and M1 and M2 of 0.35 ± 0.07 and 0.37 ± 0.04, respectively. The degree of co-localization was lower for the other organelles (Fig. 2b and c, Table S1).

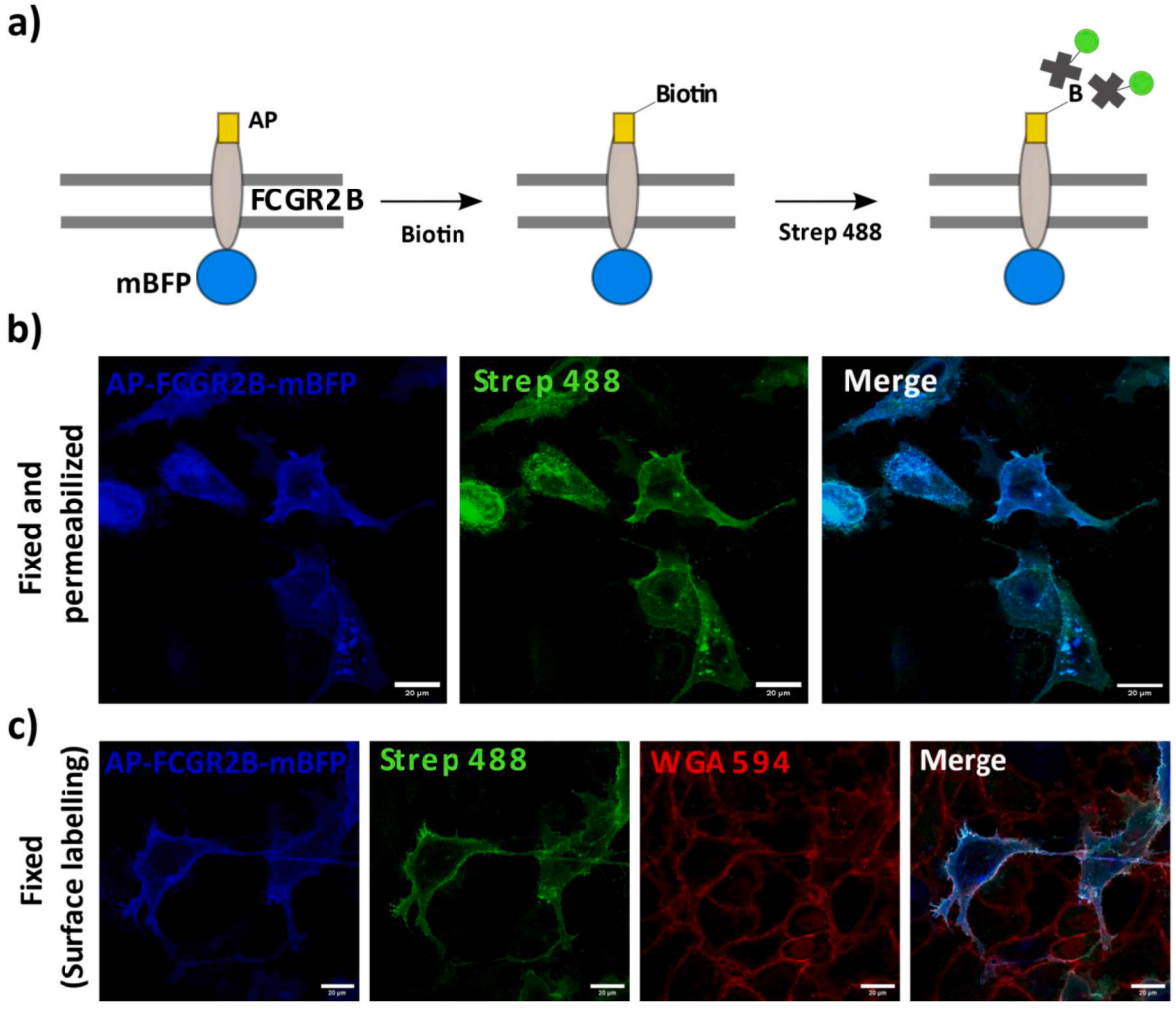

Fig. 1. Expression of AP-FCGR2B-mBFP. a) Schematic representation of the site-specific biotinylation of AP and labeling with streptavidin Alexa Fluor™ 488. **b,c)** Representative confocal images of T24 cells transfected for 24 h with AP-FCGR2B-mBFP and Bir A plasmids. In **(b)** cells were fixed, permeabilized and labeled with Alexa Fluor™ 488 conjugated to streptavidin. In **(c)** cells were only fixed and labeled with Alexa Fluor™ 488 conjugated with streptavidin and WGA Alexa Fluor™ 594. Scale bar 20 μm.

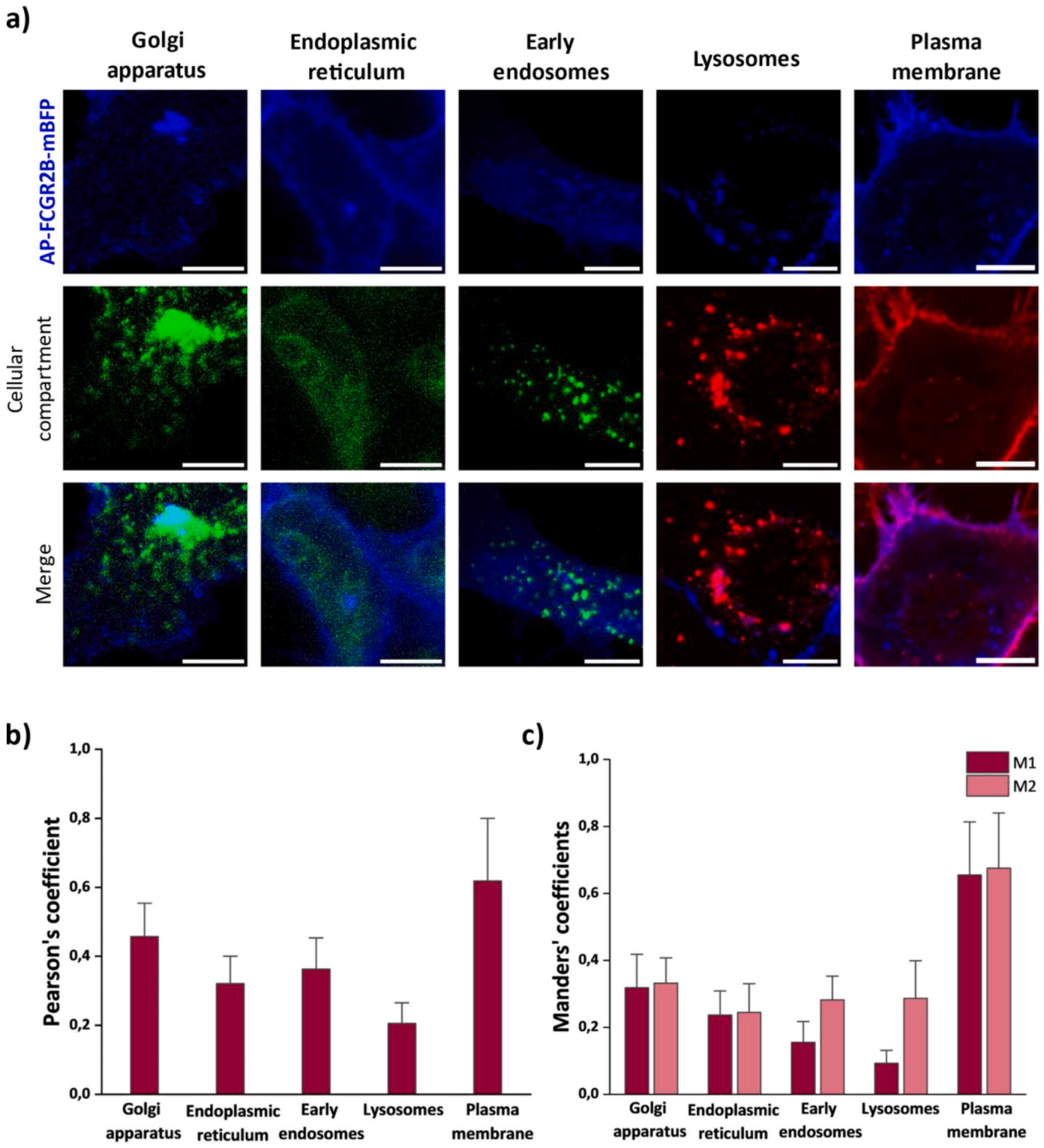

Fig. 2. FcγRIIB co-localization with cellular compartments. a) Representative confocal images of living T24 cells transfected with AP-FCGR2B-mBFP and mEmerald-TGNP-N-10, mEmerald-Calnexin-N-14 and GFP-EEA1wt plasmids to label Golgi apparatus, endoplasmic reticulum and early endosomes, respectively. To label lysosomes, cells were incubated with LysoTracker™ Red DND-99 for 30 min before acquisition. To label the plasma membrane cells transfected with AP-FCGR2B-mBFP were stained with WGA Alexa Fluor™ 594 for 30 min before acquisition. n > 30 cells from 3 independent experiments. Scale bar 10 μm. **b)** Pearson's coefficient histogram. **c)** Manders' colocalization coefficients histogram (M1, fraction of FcγRIIB overlapping with cellular marker; M2, fraction of cellular marker overlapping with FcγRIIB). Error bars, standard error (SE). (For interpretation of the references to color in this figure legend, the reader is referred to the Web version of this article.)

3.2. Cellular localization of FcRn

A construct analogous to AP-FCGR2B-mBFP was developed also in the case of the FcRn (AP-FcRn-mBFP) and its potential labeling with streptavidin Alexa Fluor™ 488 was tested under fixation and permeabilization, or fixation only, conditions (Fig. 3a–c). As the binding of β2M to FcRn appears to be an important factor for the surface expression of the FcRn [43,44], cells were co-transfected also with β2M.

We observed an overlay between the AP-FcRn-mBFP and streptavidin Alexa Fluor™ 488 labeling only in cells that had been fixed and permeabilized (Fig. 3b and c). Moreover, no colocalization was detected between the cell membrane labeled with WGA Alexa Fluor™ 594 and the receptor (Fig. 3c), indicating that the receptor was not translocated to the cell membrane.

To ensure that the exogenous tags (AP and mBFP) were not interfering with the correct folding of the protein, cells were co-transfected with plasmids containing the FcRn protein without tags (OriGene-FcRn) and β2M, and then immunolabeled with the fluorescent anti-FcRn488 antibody, whose specificity was successfully validated, in contrast to the results obtained with another widely used commercial antibody (Fig. S1–S3). FcRn appeared to be present in the cytoplasm of the cells, but was still not detectable on the cell surface, as in the experiments using the tagged construct (Fig. S1). This result indicated that the tags (AP or mBFP) were not responsible for the lack of translocation of the FcRn to the cell membrane.

To assess proper β2M expression, flow cytometry was performed in T24 cells co-transfected with AP-FcRn-mBFP and β2M (Fig. 4). FcRn was labeled with Alexa Fluor™ 488 conjugated to streptavidin and β2M with an anti-β2M primary antibody followed by an Alexa Fluor™ 647 secondary antibody. The forward (FSC-A) and side scatter (SSC-A) profile showed similar population distribution in both not labeled and labeled cells (Fig. 4 a and b left panel). Using the same gating strategy, we confirmed that the analyzed cell populations were comparable. Within this population, comparison of FL1-A (green) and FL4-A (red) fluorescence revealed a strong overlap of signals, indicating that cells expressing FcRn (green) also expressed comparable high levels of β2M (red) (Fig. 4b).

As an additional control, β2M was genetically engineered with an mCherry tag and co-transfected it in T24 cells with AP–FcRn–mBFP. Confocal microscopy imaging revealed a clear overlay of the mCherry-tagged β2M and the FcRn labeled with Alexa Fluor™ 488 conjugated to streptavidin (Fig. 4c), further validating the co-expression and intracellular association of the two proteins.

We then characterized the potential co-localization of AP-FcRn-

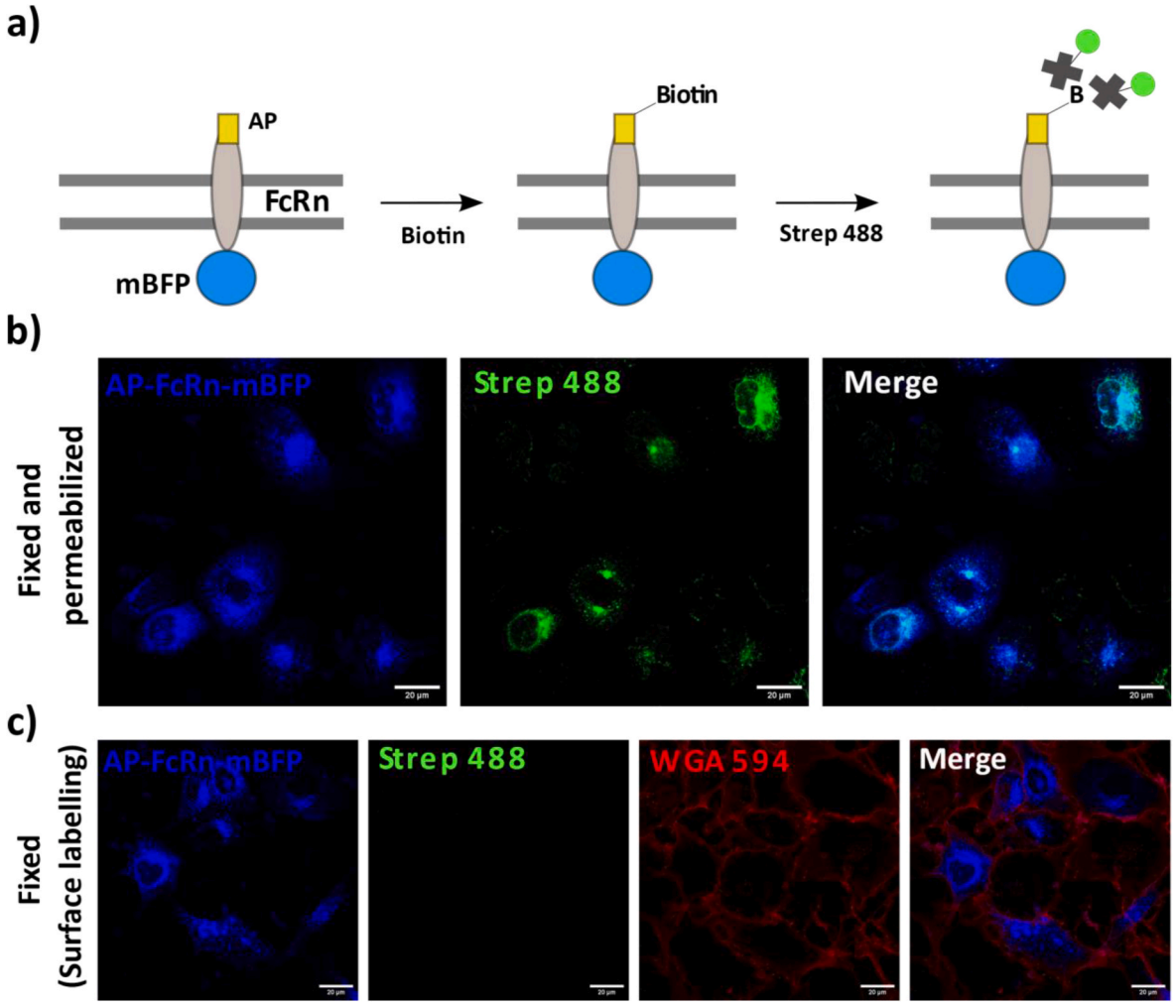

Fig. 3. Expression of AP-FcRn-mBFP. a) Site-specific biotinylation of AP and surface labeling with streptavidin Alexa Fluor™ 488 scheme. **(b, c)** Representative confocal image from T24 cells transfected with AP-FcRn-mBFP, Bir A and β2M plasmids, labeled with Alexa Fluor™ 488 conjugated with streptavidin. In **(b)** cells were fixed, permeabilized and labeled with Alexa Fluor™ 488 conjugated to streptavidin. In **(c)** cells were only fixed and labeled with Alexa Fluor™ 488 conjugated with streptavidin and WGA Alexa Fluor™ 594. Scale bar 20 μm.

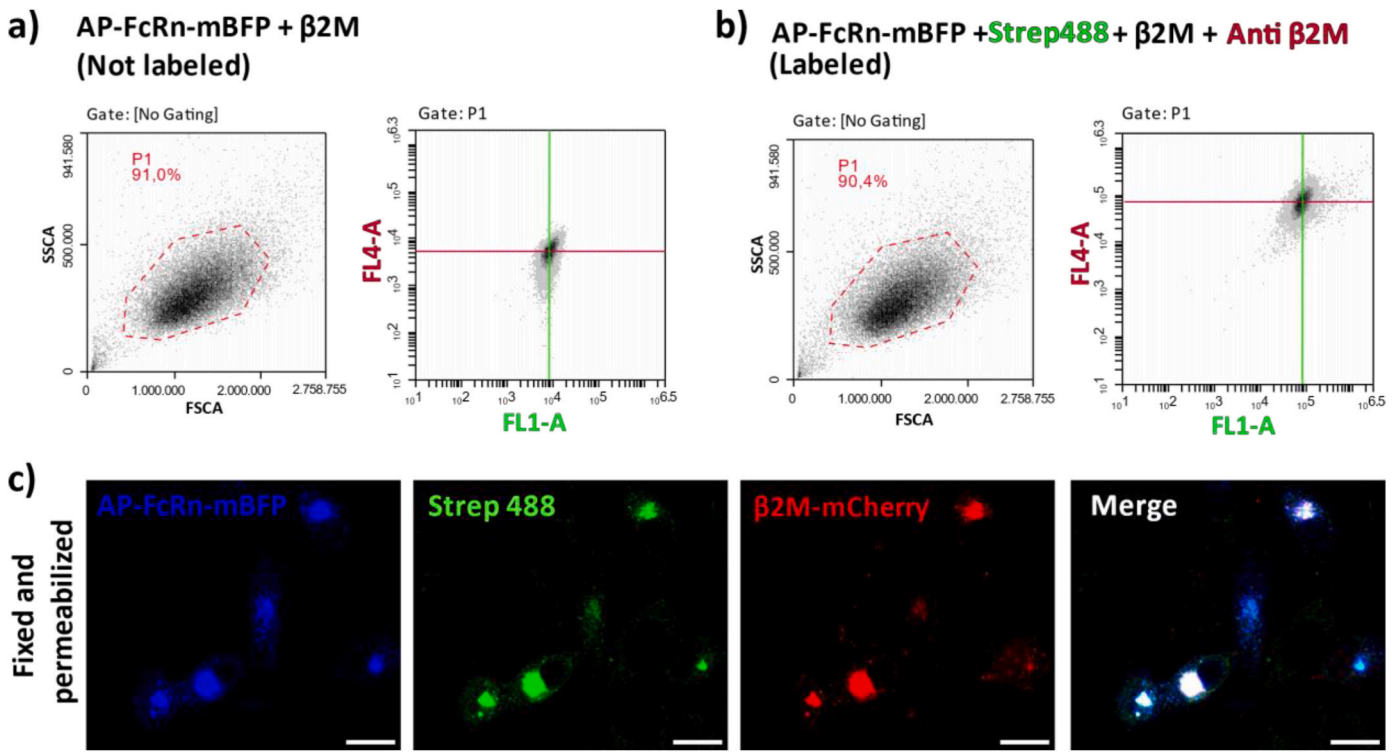

Fig. 4. Co-expression and colocalization of FcRn and β2M. a) Flow cytometry analysis of T24 cells co-transfected with AP–FcRn–mBFP, Bir A and β2M without fluorescent labeling, showing the forward (FSC-A) and side scatter (SSC-A) profile (left) and fluorescence gating (right). b) Flow cytometry analysis of labeled cells: FcRn detected with Alexa Fluor™ 488 conjugated with streptavidin (green, FL1-A) and β2M detected with anti-β2M primary antibody and Alexa Fluor™ 647 secondary antibody (red, FL4-A). The fluorescence intensities of green (FcRn) and red (β2M) channels overlap, confirming co-expression. c) Representative confocal image from T24 cells transfected with AP-FcRn-mBFP, Bir A and β2M-mCherry plasmids, labeled with Alexa Fluor™ 488 conjugated with streptavidin. Scale bar 20 μm. (For interpretation of the references to color in this figure legend, the reader is referred to the Web version of this article.)

mBFP with different cellular markers (Fig. 5a–c). In contrast to FcγRIIB, the FcRn was predominantly found in the Golgi apparatus (Pearson's coefficient = 0.76 ± 0.05; Manders' coefficients M1 = 0.83 ± 0.03, M2 = 0.75 ± 0.04), with minimal presence in other compartments (Fig. 5b and c, Table S2).

3.3. Single molecule tracking of FcγRIIB and FcRn

T24 cells were co-transfected with either AP-FCGR2B-mBFP and Bir A, or AP-FcRn-mBFP, Bir A and β2M, and incubated with streptavidin conjugated with QDs to follow the dynamics of individual receptor proteins on the surface of living cells (Fig. 6a–d and video S1).

Supplementary data related to this article can be found online at https://doi.org/10.1016/j.abb.2025.110628

Trajectories of single AP-FcRn-mBFP or AP-FCGR2B-mBFP were extrapolated from the real time recordings. The mean squared displacement (MSD) measurement of the trajectories was used and distinct parameters including diffusion coefficient *D* and confidence values were calculated (Tables 1 and 2) using the publicly available algorithms TrackMate [40] and TraJClassifier [41]. As the QDs blink, and re-linking is not always possible, some of the individually reconstructed trajectories could belong to the same molecule. In live cell experiments, single particle tracking has revealed that molecules can exhibit various motion types. These motion types are typically identified by analyzing the shape of their MSD curve. The four basic types of motion, normal diffusion, subdiffusion, directed motion or confined diffusion, have a distinct MSD curve [41,45]. A model of the MSD curve for a specific motion type, fitted to the data points, can be used to determine key parameters such as the diffusion coefficient *D*.

The FcγRIIB and FcRn displayed very different features, starting from the number of QDs detected in the single molecule experiments: around 6 (±1.4) QDs per cell in the case of FcRn in comparison to an average of 168 (±44) for the FcγRIIB (Fig. 6c and d). While a total of 2636 trajectories were analyzed for the FcγRIIB, only 96 trajectories from a comparable number of cells were analyzed for the FcRn (Tables 1 and 2).

Since sub-trajectories with different types of motion could be detected within the same trajectory, we calculated the duration of distinct sub-trajectories types over the total length of the trajectory, rather than classifying the trajectories according to the main type of motion (Fig. 6b). The analysis of FcγRIIB sub-trajectories showed that on average FcγRIIB molecules spent the majority of total trajectory time moving according to normal diffusion (~70 %), with a median diffusion coefficient (*D*) of 1.10 x 10^{-3} μm^2/s (Fig. 6e). Some FcγRIIB molecules displayed directed motion for approximately 6 % of the total trajectory length, with a median *D* of 1.76 x 10^{-3} μm^2/s and a mean velocity (v) of 0.097 μm/s, indicating that this protein can be internalized and actively transported. This velocity was comparable to the lower range of reported dynein speeds (0,1 < v < 1 μm/s) [46,47]. Few FcγRIIB molecules were undergoing sub-diffusion for nearly 7 % of time, with a median *D* of 2.48 x 10^{-4} μm^2/s and an average anomalous exponent (α) of 0.36 (α < 1 corresponds to subdiffusion), and few were spending about 6 % of the time in an immobile state (D < 10^{-4} μm^2/s) [48]. It appears that FcγRIIB barely undergoes confined motion, with a median *D* of 5.45 x 10^{-3} μm^2/s for the confined sub-trajectories, and an average confinement radius of 61 nm (Fig. 6e and Table 1).

In contrast, approximately more than a half of FcRn receptors on the cell surface were immobile most of the time (~55 %), undergoing sub-diffusion (<30 %) or confined motion (<10 %). The fraction of trajectories classified as sub-diffusive displayed a median *D* of 2.75 x 10^{-4} μm^2/s and an average α of 0.17, this suggested that the particle's movement is restricted and heavily constrained. We did not find any sub-trajectory that could be classified as normal diffusion or directed

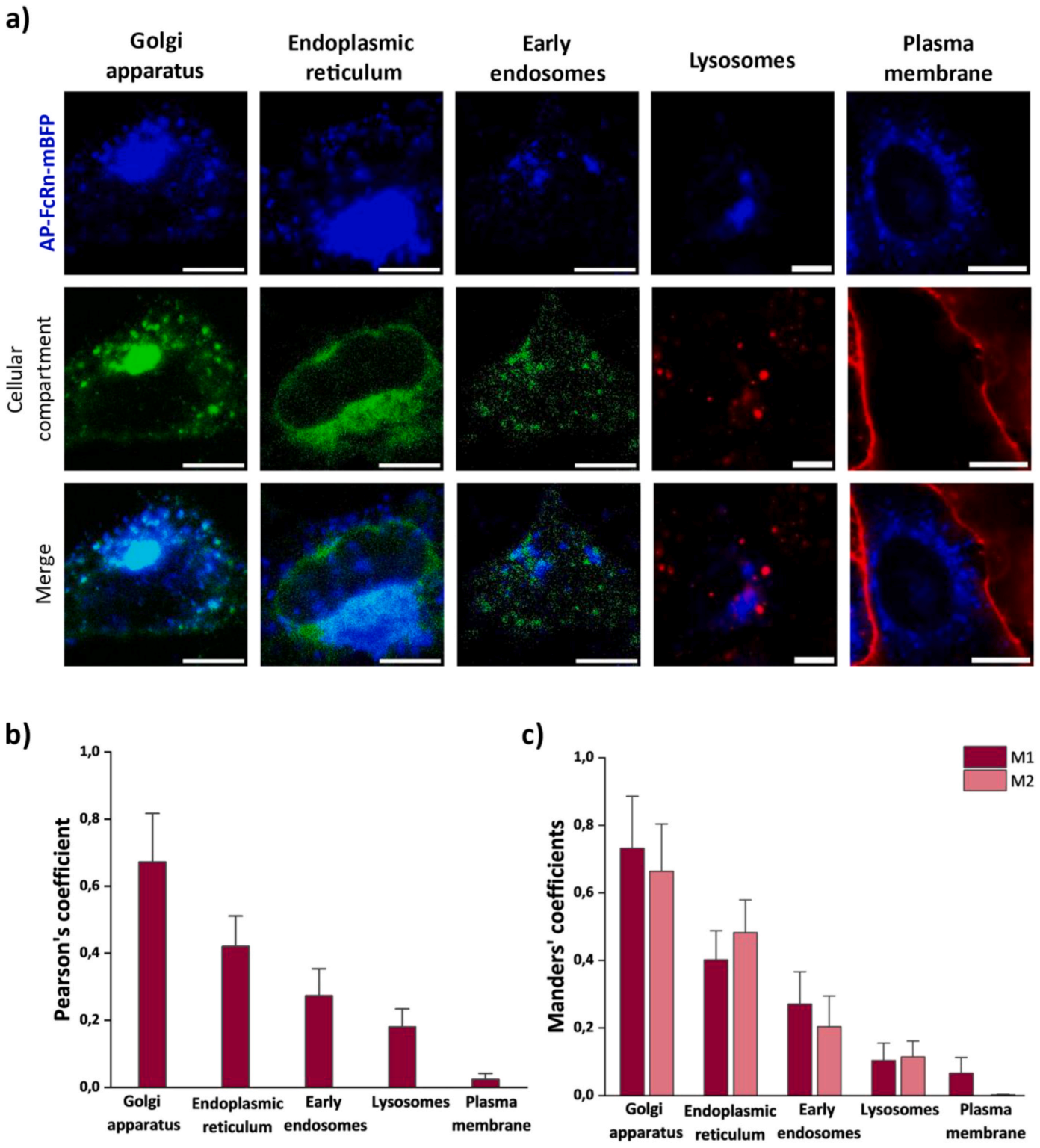

Fig. 5. FcRn co-localization with cellular compartments. **a)** Representative confocal images of T24 cells transfected with the AP-FcRn-mBFP and β2M plasmids. To label Golgi apparatus, endoplasmic reticulum and early endosomes, cells were co-transfected with mEmerald-TGNP-N-10, mEmerald-Calnexin-N-14 and GFP-EEA1wt plasmids, respectively. To label lysosomes, cells were incubated with LysoTracker™ Red DND-99 for 30 min before acquisition. To label the plasma membrane cells were stained with WGA Alexa Fluor™ 594 for 30 min before acquisition. n > 30 cells from 3 independent experiments. Scale bar 10 μm. **b)** Pearson's coefficient histogram. **c)** Manders' colocalization coefficients histogram (M1, fraction of FcRn overlapping with cellular marker; M2, fraction of cellular marker overlapping with FcRn). Error bars, SE. (For interpretation of the references to color in this figure legend, the reader is referred to the Web version of this article.)

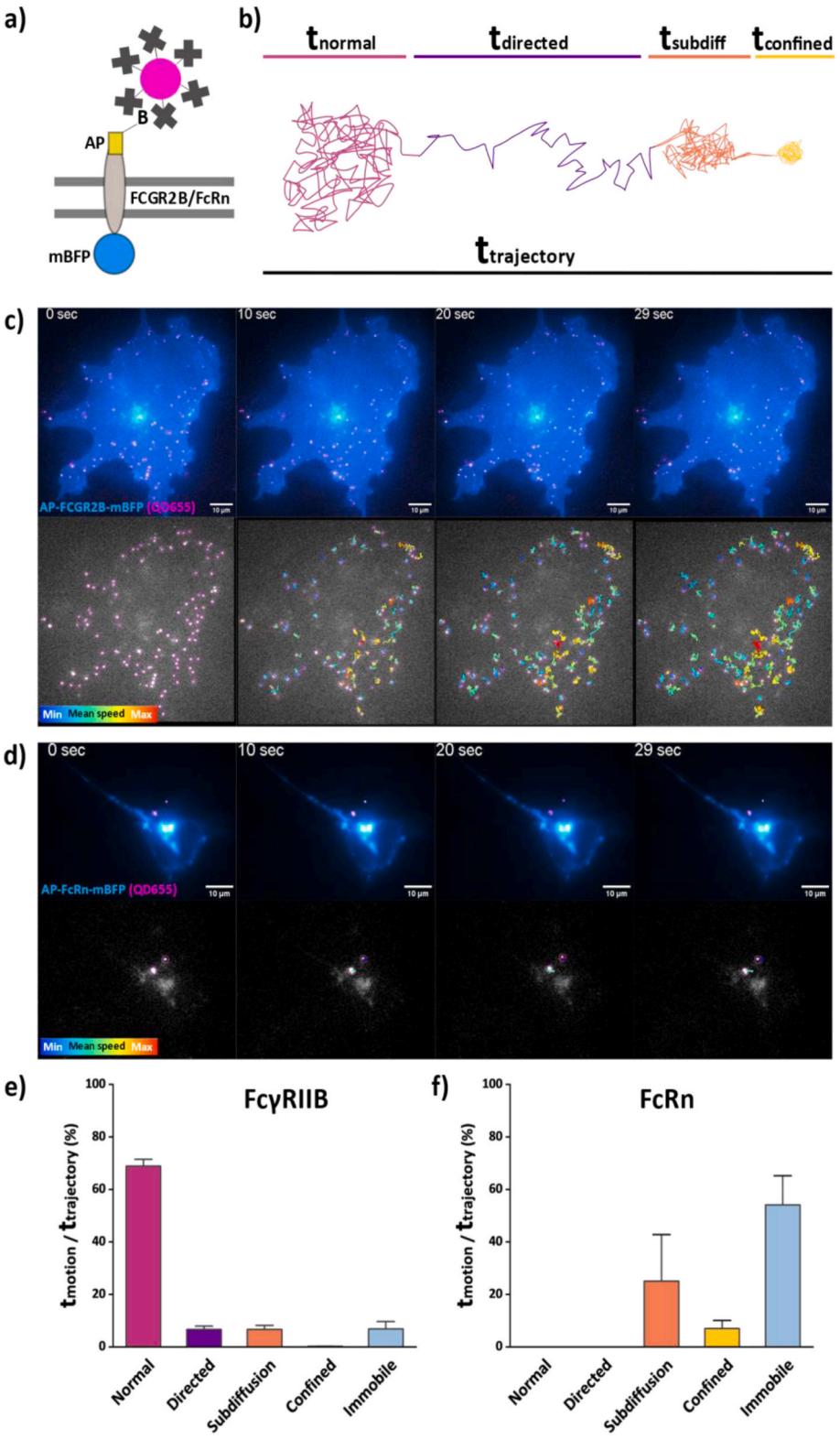

Fig. 6. SMT of FcγRIIB and FcRn. a) Schematic representation of site-specific biotinylation of AP tag and surface labeling with Qdot™ 655 streptavidin for FcγRIIB or FcRn receptors. **b)** Representation of sub-trajectories associated to different types of motion identified within the same trajectory of a receptor molecule. **c)** Representative images of T24 living cells transfected with AP-FCGR2B-mBFP and Bir A, labeled with Qdot™ 655 streptavidin. The color of the trajectories indicates the mean speed of the molecules. n > 10 cells from 5 independent experiments. **d)** Living cells transfected with AP-FcRn-mBFP, Bir A and β2M, labeled with Qdot™ 655 streptavidin. n > 10 cells from 5 independent experiments. **e), f)** Plot of the average sub-trajectory length associated to a certain type of motion (t_{motion}) in relation to the total trajectory length ($t_{trajectory}$) for the two Fc receptors. Error bars, SE. Scale bar 10 μm. (For interpretation of the references to color in this figure legend, the reader is referred to the Web version of this article.)

Table 1
FcγRIIB diffusion data. Trajectories were extrapolated from 30s recordings of T24 living cells transfected with AP-FCGR2B-mBFP and Bir A and labeled with Qdot™ 655 streptavidin conjugate. Only trajectories with a minimum of 30 consecutive steps were considered for the analysis. Diffusion coefficients (*D*) are reported as median values, as distributed over different orders of magnitude. The rest of the values are reported as average ± SE. It should be highlighted that the values of the parameters related to the accuracy of the model (confidence, MSD ratio and fractal dimension) were within the range expected for each type of motion [36]. This supported the robustness of the obtained results (Tables 1 and 2).

	FCγRIIB				
	Normal	Directed	Subdiffusion	Confined	Immobile
D ($\mu m^2/s$)	1.10 x 10^{-3}	1.76 x 10^{-3}	2.48 x 10^{-4}	5.45 x 10^{-3}	$<10^{-4}$
Velocity (μm/s)	–	0.097 ± 0.003	–	–	–
Exponent α	–	–	0.36 ± 0.009	–	–
Confinement radius (μm)	–	–	–	0.061 ± 0.024	–
Total number of sub-trajectories	1720	414	278	17	207
Confidence	0.70 ± 0.001	0.74 ± 0.003	0.69 ± 0.004	0.7 ± 0.026	0.72 ± 0.003
MSD ratio	0.009 ± 0.004	−0.05 ± 0.002	0.48 ± 0.057	0.37 ± 0.08	0.49 ± 0.02
Fractal dimension	1.78 ± 0.004	1.32 ± 0.004	2.31 ± 0.015	2.83 ± 0.14	2.43 ± 0.02

Table 2
FcRn diffusion data. Trajectories were extrapolated from 30s recordings of T24 living cells transfected with AP-FcRn-mBFP, Bir A, β2M, and labeled with Qdot™ 655 streptavidin conjugate. As described for Table 1, only trajectories with a minimum of 30 consecutive steps were considered for the analysis. Diffusion coefficients (*D*) are reported as median values. The rest of the values are reported as average ± SE.

	FcRn				
	Normal	Directed	Subdiffusion	Confined	Immobile
D ($\mu m^2/s$)	0	0	2.75 x 10^{-4}	3.56 x 10^{-4}	$<10^{-4}$
Velocity (μm/s)	–	0	–	–	–
Exponent α	–	–	0.17 ± 0.035	–	–
Confinement radius (μm)	–	–	–	0.034 ± 0.009	–
Total number of sub-trajectories	0	0	26	7	63
Confidence	–	–	0.70 ± 0.009	0.73 ± 0.021	0.75 ± 0.008
MSD ratio	–	–	0.68 ± 0.073	0.58 ± 0.098	0.97 ± 0.06
Fractal dimension	–	–	2.61 ± 0.07	3.29 ± 0.157	3.08 ± 0.07

motion (Fig. 6f and Table 2).

To ascertain if the presence of antibodies from the FBS could have an impact on the FcRn behavior, SMT experiments were performed also in FBS free medium (Fig. S5). We did not detect any significant change in FcRn number or dynamics with respect to the complete medium condition.

4. Discussion

Currently, monoclonal antibodies (mAbs), particularly immunoglobulin G (IgG), represent the predominant class of therapeutic antibodies in clinical use. Nasal administration of therapeutic antibodies is emerging as a promising, non-invasive strategy to bypass the blood-brain barrier (BBB). Prior research has demonstrated that full-length IgG can be transported from the nasal cavity to the brain via the olfactory mucosa [49–52]. Several potential uptake pathways—such as intracellular, paracellular and diffusion-based mechanisms—have been suggested for enabling CNS delivery [53,54]. However, the molecular mechanisms underlying this process and the specific receptors involved in facilitating IgG transport remain poorly understood. Among the proposed mechanisms, receptor-mediated transcytosis (RMT) is a leading candidate for IgG transport across the olfactory epithelium [55]. FcRn and FcγRIIB have been suggested as potential key players in IgG trafficking. FcRn appears to be involved in the bidirectional transport of IgGs across polarized cell layers as those found in the placenta [14], epithelial cells that line mucosal surfaces [56] and other cell types and tissues [22]. FcRn is also expressed in the BBB but most likely related with the efflux transport [44]. Conversely, other studies suggest that the FcRn is not involved in the transport of IgGs in brain endothelial cells [24], or in the distribution of IgGs in rodent brain [57]. Another study in mice showed that neither the FcRn, nor the FcγRIIB, seemed to be involved in the IgGs transport [25]. The role of these receptors in IgG transport to the brain remains controversial, with several studies yielding conflicting results.

With these premises, we aimed at determining and comparing the cellular distribution and dynamics of FcRn and FcγRIIB in a simple cellular model, a basic defragmentation step still necessary for a better understanding of their complex role in IgG binding and trafficking.

Our findings align with previous studies reporting that only 4–7 % of endogenous FcRn is present on the cell surface [58], supporting the hypothesis that FcRn predominantly resides in intracellular compartments. Consistent with this, our experimental data indicate that FcRn is almost entirely retained intracellularly (nearly 100 %) under our conditions, with surface expression appearing even lower than previously reported [58]. This is also in part consistent with a previous study showing that, in the absence of β2M, FcRn remains sequestered in the ER (in this study however this result was not quantitatively measured) [44]. In another study [58], the degree of co-localization of endogenous FcRn with endosomes (Pearson's coefficient >0.6) was found higher than with the Golgi apparatus (Pearson's coefficient ~ 0.5). In our experiments FcRn co-localized mostly with Golgi (Pearson's coefficient ~ 0.8), both in the presence or the absence of β2M. While the high abundance of FcRn in this organelle can be a consequence of overexpression, it is unclear why FcRn did not proportionally accumulate in the ER, or at the endosomal level. On the other hand, we observed that FcγRIIB was mostly detected on the cell surface, in agreement with other previous studies [59,60].

To study the mobility and potential active transport of these receptors, a fundamental process to guarantee IgG trafficking and recycling, we employed single molecule imaging and tracking. FcγRIIB molecules displayed a much higher mobility than those few FcRn molecules found on the cell membrane, which were immobile or displayed confined mobility. As the very same tags were introduced in the FcγRIIB and FcRn constructs (each incorporating an AP tag at the N-terminus after the signal peptide, and a mBFP fused to the C-terminus), the dramatic differences in mobility and cellular distribution between the two proteins appear independent from the genetically engineered modifications. According to the Saffman-Delbrück and subsequent models, differences in diffusion rates between membrane proteins can be in part dependent on the lateral radius (R) of their transmembrane domain, following a logarithmic or non-logarithmic inverse relation ($D \propto \ln(1/R)$ [61] or $D \propto 1/R$ [62]. It seems however unlikely that the distinct diffusion features of FcγRIIB and FcRn can be a consequence of this relation, or of their overall size, as both proteins have a single spanning transmembrane domain of similar size (22 amino acids in FcγRIIB, 23 in FcRn) and consist of approximately 300 amino acids. Our data on the high mobility of FcγRIIB are in agreement with a previous study in a model B-cell line [59]. Some events of intracellular directed motion, at a

speed compatible with that of the molecular motor dynein [46,47], were observed in the case of FcγRIIB. The restricted mobility found for FcRn may be a consequence of direct or indirect interaction with cytoskeletal elements, limiting its diffusion and potentially influencing its role in receptor-mediated transport [63,64]. The low abundance of FcRn on the cell surface, together with its reduced mobility and not frequent internalization, do not appear as the ideal premise to efficiently bind extracellular IgGs and promote their internalization and trafficking, at least in cultured epithelial-like cells.

FcγRIIB binds monomeric IgG weakly (micromolar KD) compared to other Fcγ receptors observed in previous studies [65,66] and primarily engages immune complexes or multivalent IgG to trigger signaling or internalization. While this limits its role in monomeric IgG trafficking, weak binding may actually benefit transcytosis, a type of transport that requires reversible interactions. This low affinity could be advantageous for therapeutic antibodies, which are present at higher-than-physiological levels, allowing efficient binding, internalization, directional transport and release of IgGs. A too stable binding would indeed work against the release, limiting the probability of dissociation events.

Clearly defining the cellular distribution and the mobility of FcRn or FcγRIIB on the plasma membrane is propaedeutic to a clear understanding of RMT processes in the context of N2B delivery. FcRn and FcγRIIB displayed very different behaviors, from the number of molecules capable of reaching the cell surface, to the type of motion extrapolated from their trajectories. The data indicate that FcγRIIB, more than FcRn, displays features that could be compatible with the internalization and trafficking of IgGs.

Discrepancies between human and murine studies regarding FcγRIIB and FcRn in IgG trafficking highlight the complexity of this field. Contributing factors may include species-specific differences in receptor biology, variability in receptor expression, and differences in experimental systems. Murine studies using knockout models for FcRn or FcγRIIB have provided valuable insights in vivo, whereas human-based studies show variable results depending on the cell model. Ishikawa et al. demonstrated that FcγRIIB contributes to maternal IgG transport in HUVECs [27], whereas Ruano-Salguero and Lee reported FcRn-independent IgG transport across human induced pluripotent stem cells (iBECs) [24]. Additionally, Zhu et al. found that FcRn is largely sequestered in the endoplasmic reticulum in FO-1 melanoma cells lacking β2-microglobulin [44], highlighting cell-type–dependent receptor localization. These findings underscore the need for multiple model systems and further mechanistic studies in physiologically relevant human contexts.

Although our data contribute to elucidate basic features of FcγRIIB (isoform 1) and FcRn, certain limitations remain, which also point to important directions for future research: the SMT setup used in this study is not suitable for polarized cell cultures, limiting the physiological relevance of receptor dynamics in epithelial or endothelial barriers. We focused solely on the FcγRIIB1 isoform, though FcγRIIB2, with its distinct structural and functional properties, would also be important to investigate in future studies. Additionally, receptor–ligand interactions were not assessed here, but studying their effects on receptor behavior will be an imperative future objective. Finally, it is important to emphasize that the physiological roles of both FcγRIIB and FcRn, particularly in non-immune tissues, remain only partially elucidated. As new evidence emerges, current paradigms regarding their function may need to be revised or expanded, underscoring the importance of continued investigation into their biology.

CRediT authorship contribution statement

Marta Rojas-Rodríguez: Writing – original draft, Methodology, Investigation, Formal analysis, Data curation, Conceptualization. **Francesco Saverio Pavone:** Supervision, Resources. **Martino Calamai:** Writing – review & editing, Supervision, Resources, Project administration, Methodology, Investigation, Funding acquisition, Formal analysis, Data curation, Conceptualization.

Declaration of interest

The authors declare no competing interests.

Acknowledgments

This project has received funding from the European Union's Horizon 2020 research and innovation program under the Marie Skłodowska-Curie grant agreement No 956977.

Appendix A. Supplementary data

Supplementary data to this article can be found online at https://doi.org/10.1016/j.abb.2025.110628.

Data availability

Data will be made available on request.

References

[1] M. Pyzik, K.M.K. Sand, J.J. Hubbard, J.T. Andersen, I. Sandlie, R.S. Blumberg, The neonatal Fc receptor (FcRn): a misnomer? Front. Immunol. 10 (2019).
[2] M.D. Hulett, P.M. Hogarth, in: F.J.B.T.-A. Dixon (Ed.), Molecular Basis of Fc Receptor Function, Academic Press, 1994, pp. 1–127.
[3] D.G. Brooks, W.Q. Qiu, A.D. Luster, J.V. Ravetch, Structure and expression of human IgG FcRII(CD32). Functional heterogeneity is encoded by the alternatively spliced products of multiple genes, J. Exp. Med. 170 (1989) 1369–1385.
[4] M.J. Aman, A.C. Tosello-Trampont, K. Ravichandran, Fc gamma RIIB1/SHIP-mediated inhibitory signaling in B cells involves lipid rafts, J. Biol. Chem. 276 (2001) 46371–46378.
[5] J.C. Anania, A.M. Chenoweth, B.D. Wines, P.M. Hogarth, The human FcγRII (CD32) family of leukocyte FcR in health and disease, Front. Immunol. 10 (2019) 464.
[6] K.G.C. Smith, M.R. Clatworthy, FcgammaRIIB in autoimmunity and infection: evolutionary and therapeutic implications, Nat. Rev. Immunol. 10 (2010) 328–343.
[7] S.Y. Chu, H.M. Horton, E. Pong, I.W.L. Leung, H. Chen, D.-H. Nguyen, C. Bautista, U.S. Muchhal, M.J. Bernett, G.L. Moore, D.E. Szymkowski, J.R. Desjarlais, Reduction of total IgE by targeted coengagement of IgE B-cell receptor and FcγRIIb with Fc-engineered antibody, J. Allergy Clin. Immunol. 129 (2012) 1102–1115.
[8] O.T. Burton, A. Epp, M.E. Fanny, S.J. Miller, A.J. Stranks, J.E. Teague, R.A. Clark, M. van de Rijn, H.C. Oettgen, Tissue-Specific expression of the low-affinity IgG receptor, FcγRIIb, on human mast cells, Front. Immunol. 9 (2018).
[9] Y.C. Xia, N.S. Redhu, L.M. Moir, C. Koziol-White, A.J. Ammit, L. Al-Alwan, B. Camoretti-Mercado, R.L. Clifford, Pro-inflammatory and immunomodulatory functions of airway smooth muscle: emerging concepts, Pulm. Pharmacol. Ther. 26 (2013) 64–74.
[10] D.D. Sedmak, D.H. Davis, U. Singh, J.G. van de Winkel, C.L. Anderson, Expression of IgG Fc receptor antigens in placenta and on endothelial cells in humans. An immunohistochemical study, Am. J. Pathol. 138 (1991) 175–181.
[11] T. Mishima, G. Kurasawa, G. Ishikawa, M. Mori, Y. Kawahigashi, T. Ishikawa, S.-S. Luo, T. Takizawa, T. Goto, S. Matsubara, T. Takeshita, J.M. Robinson, T. Takizawa, Endothelial expression of Fc gamma receptor IIb in the full-term human placenta, Placenta 28 (2007) 170–174.
[12] S.A. Mousavi, M. Sporstøl, C. Fladeby, R. Kjeken, N. Barois, T. Berg, Receptor-mediated endocytosis of immune complexes in rat liver sinusoidal endothelial cells is mediated by FcγRIIb2, Hepatology 46 (2007) 871–884.
[13] S. Ladel, F. Maigler, J. Flamm, P. Schlossbauer, A. Handl, R. Hermann, H. Herzog, T. Hummel, B. Mizaikoff, K. Schindowski, Impact of glycosylation and species origin on the uptake and permeation of IgGs through the nasal airway Mucosa, Pharmaceutics 12 (2020).
[14] N.E. Simister, K.E. Mostov, An Fc receptor structurally related to MHC class I antigens, Nature 337 (1989) 184–187.
[15] R. Rodewald, pH-dependent binding of immunoglobulins to intestinal cells of the neonatal rat, J. Cell Biol. 71 (1976) 666–669.
[16] B.L. Dickinson, K. Badizadegan, Z. Wu, J.C. Ahouse, X. Zhu, N.E. Simister, R. S. Blumberg, W.I. Lencer, Bidirectional FcRn-dependent IgG transport in a polarized human intestinal epithelial cell line, J. Clin. Investig. 104 (1999) 903–911.
[17] P.J. Hornby, P.R. Cooper, C. Kliwinski, E. Ragwan, J.R. Mabus, B. Harman, S. Thompson, A.L. Kauffman, Z. Yan, S.H. Tam, H. Dorai, G.D. Powers, J. Giles-Komar, Human and non-human primate intestinal FcRn expression and immunoglobulin G transcytosis, Pharm. Res. 31 (2014) 908–922.
[18] J.-P. Haymann, J.-P. Levraud, S. Bouet, V. Kappes, J. Hagège, G. Nguyen, Y. Xu, E. Rondeau, J.-D. Sraer, Characterization and localization of the neonatal Fc receptor in adult human kidney, J. Am. Soc. Nephrol. 11 (2000) 632–639.

[19] R.S. Blumberg, T. Koss, C.M. Story, D. Barisani, J. Polischuk, A. Lipin, L. Pablo, R. Green, N.E. Simister, A major histocompatibility complex class I-related Fc receptor for IgG on rat hepatocytes, J. Clin. Investig. 95 (1995) 2397–2402.

[20] F. Schlachetzki, C. Zhu, W.M. Pardridge, Expression of the neonatal Fc receptor (FcRn) at the blood-brain barrier, J. Neurochem. 81 (2002) 203–206.

[21] H.P. Montoyo, C. Vaccaro, M. Hafner, R.J. Ober, W. Mueller, E.S. Ward, Conditional deletion of the MHC class I-related receptor FcRn reveals the sites of IgG homeostasis in mice, Proc. Natl. Acad. Sci. U. S. A 106 (2009) 2788–2793.

[22] D.C. Roopenian, S. Akilesh, FcRn: the neonatal Fc receptor comes of age, Nat. Rev. Immunol. 7 (2007) 715–725.

[23] P.R. Cooper, G.J. Ciambrone, C.M. Kliwinski, E. Maze, L. Johnson, Q. Li, Y. Feng, P. J. Hornby, Efflux of monoclonal antibodies from rat brain by neonatal Fc receptor, FcRn, Brain Res. 1534 (2013) 13–21.

[24] J.S. Ruano-Salguero, K.H. Lee, Antibody transcytosis across brain endothelial-like cells occurs nonspecifically and independent of FcRn, Sci. Rep. 10 (2020) 3685.

[25] L. Abuqayyas, J.P. Balthasar, Investigation of the role of FcγR and FcRn in mAb distribution to the brain, Mol. Pharm. 10 (2013) 1505–1513.

[26] N. Chen, W. Wang, S. Fauty, Y. Fang, L. Hamuro, A. Hussain, T. Prueksaritanont, The effect of the neonatal Fc receptor on human IgG biodistribution in mice, mAbs 6 (2014) 502–508.

[27] T. Ishikawa, T. Takizawa, J. Iwaki, T. Mishima, K. Ui-Tei, T. Takeshita, S. Matsubara, T. Takizawa, Fc gamma receptor IIb participates in maternal IgG trafficking of human placental endothelial cells, Int. J. Mol. Med. 35 (2015) 1273–1289.

[28] S. Borghi, S. Bournazos, N.K. Thulin, C. Li, A. Gajewski, R.W. Sherwood, S. Zhang, E. Harris, P. Jagannathan, L.-X. Wang, J. V Ravetch, T.T. Wang, FcRn, but not FcγRs, drives maternal-fetal transplacental transport of human IgG antibodies, Proc. Natl. Acad. Sci. 117 (2020) 12943–12951.

[29] O.M. Subach, P.J. Cranfill, M.W. Davidson, V.V. Verkhusha, An enhanced monomeric blue fluorescent protein with the high chemical stability of the chromophore, PLoS One 6 (2011) 1–9.

[30] N. Parenti, A. Del Grosso, C. Antoni, M. Cecchini, R. Corradetti, F.S. Pavone, M. Calamai, Direct imaging of APP proteolysis in living cells, PeerJ 2017 (2017) 1–22.

[31] D. Beckett, E. Kovaleva, P.J. Schatz, A minimal peptide substrate in biotin holoenzyme synthetase-catalyzed biotinylation, Protein Sci. 8 (1999) 921–929.

[32] M. Howarth, K. Takao, Y. Hayashi, A.Y. Ting, Targeting quantum dots to surface proteins in living cells with biotin ligase, Proc. Natl. Acad. Sci. U. S. A 102 (2005) 7583–7588.

[33] D.C. Lawe, V. Patki, R. Heller-Harrison, D. Lambright, S. Corvera, The FYVE domain of early endosome antigen 1 is required for both phosphatidylinositol 3-phosphate and Rab5 binding. Critical role of this dual interaction for endosomal localization, J. Biol. Chem. 275 (2000) 3699–3705.

[34] S. Bolte, F.P. Cordelières, A guided tour into subcellular colocalization analysis in light microscopy, J. Microsc. 224 (2006) 213–232.

[35] K. Pearson, A. Lee, On the laws of inheritance in man: I. Inheritance of physical characters, Biometrika 2 (1903) 357–462.

[36] E.M. Manders, J. Stap, G.J. Brakenhoff, R. van Driel, J.A. Aten, Dynamics of three-dimensional replication patterns during the S-phase, analysed by double labelling of DNA and confocal microscopy, J. Cell Sci. 103 (Pt 3) (1992) 857–862.

[37] H. Bannai, S. Lévi, C. Schweizer, M. Dahan, A. Triller, Imaging the lateral diffusion of membrane molecules with quantum dots, Nat. Protoc. 1 (2007) 2628–2634.

[38] Dot-conjugated, T.T.Q., L. Gardini, M. Calamai, H. Hatakeyama, M. Kanzaki, M. Capitanio, and F.S. Pavone. Chapter 26. 1814.

[39] M. Calamai, F.S. Pavone, Single molecule tracking analysis reveals that the surface mobility of amyloid oligomers is driven by their conformational structure, J. Am. Chem. Soc. 133 (2011) 12001–12008.

[40] J.Y. Tinevez, N. Perry, J. Schindelin, G.M. Hoopes, G.D. Reynolds, E. Laplantine, S. Y. Bednarek, S.L. Shorte, K.W. Eliceiri, TrackMate: an open and extensible platform for single-particle tracking, Methods 115 (2017) 80–90.

[41] T. Wagner, A. Kroll, C.R. Haramagatti, H.G. Lipinski, M. Wiemann, Classification and segmentation of nanoparticle diffusion trajectories in cellular micro environments, PLoS One 12 (2017) 1–20.

[42] C. Capitini, F. Feo, A. Caciotti, R. Tonin, M. Lulli, D. Coviello, R. Guerrini, M. Calamai, A. Morrone, Fluorescent in situ staining and flow cytometric procedures as new pre-diagnostic tests for sialidosis, GM1 gangliosidosis and niemann–pick type C, Biomedicines 10 (2022).

[43] A. Praetor, W. Hunziker, β2-microglobulin is important for cell surface expression and pH-dependent IgG binding of human FcRn, J. Cell Sci. 115 (2002) 2389–2397.

[44] X. Zhu, J. Peng, R. Raychowdhury, A. Nakajima, W.I. Lencer, R.S. Blumberg, The heavy chain of neonatal Fc receptor for IgG is sequestered in endoplasmic reticulum by forming oligomers in the absence of beta2-microglobulin association, Biochem. J. 367 (2002) 703–714.

[45] M.J. Saxton, K. Jacobson, SINGLE-PARTICLE TRACKING:Applications to membrane dynamics, Annu. Rev. Biophys. 26 (1997) 373–399.

[46] S.L. Reck-Peterson, A. Yildiz, A.P. Carter, A. Gennerich, N. Zhang, R.D. Vale, Single-molecule analysis of dynein processivity and stepping behavior, Cell 126 (2006) 335–348.

[47] J. Ando, T. Shima, R. Kanazawa, R. Shimo-Kon, A. Nakamura, M. Yamamoto, T. Kon, R. Iino, Small stepping motion of processive dynein revealed by load-free high-speed single-particle tracking, Sci. Rep. 10 (2020) 1080.

[48] T.J. Feder, I. Brust-Mascher, J.P. Slattery, B. Baird, W.W. Webb, Constrained diffusion or immobile fraction on cell surfaces: a new interpretation, Biophys. J. 70 (1996) 2767–2773.

[49] S. Cattepoel, M. Hanenberg, L. Kulic, R.M. Nitsch, Chronic intranasal treatment with an anti-Aβ(30-42) scFv antibody ameliorates amyloid pathology in a transgenic mouse model of Alzheimer's disease, PLoS One 6 (2011) e18296.

[50] V.V. Kolobov, I.A. Zakharova, V.G. Fomina, V.Y. Gorbatov, T.V. Davydova, Effect of antibodies to glutamate on caspase-3 activity in brain structures of rats with experimental Alzheimer's disease, Bull. Exp. Biol. Med. 154 (2013) 425–427.

[51] V. Pernet, Nogo-A in the visual system development and in ocular diseases, Biochim. Biophys. acta. Mol. basis Dis. 1863 (2017) 1300–1311.

[52] D. Correa, M.I. Scheuber, H. Shan, O.W. Weinmann, Y.A. Baumgartner, A. Harten, A.-S. Wahl, K.L. Skaar, M.E. Schwab, Intranasal delivery of full-length anti-Nogo-A antibody: a potential alternative route for therapeutic antibodies to central nervous system targets, Proc. Natl. Acad. Sci. 120 (2023) e2200057120.

[53] L.A. Keller, O. Merkel, A. Popp, Intranasal drug delivery: opportunities and toxicologic challenges during drug development, Drug Deliv. Transl. Res. 12 (2022) 735–757.

[54] F. Erdő, L.A. Bors, D. Farkas, Á. Bajza, S. Gizurarson, Evaluation of intranasal delivery route of drug administration for brain targeting, Brain Res. Bull. 143 (2018) 155–170.

[55] M. Fieux, S. Le Quellec, S. Bartier, A. Coste, B. Louis, C. Giroudon, M. Nourredine, E. Bequignon, FcRn as a transporter for nasal delivery of biologics: a systematic review, Int. J. Mol. Sci. 22 (2021).

[56] S. Tzaban, R.H. Massol, E. Yen, W. Hamman, S.R. Frank, L.A. Lapierre, S. H. Hansen, J.R. Goldenring, R.S. Blumberg, W.I. Lencer, The recycling and transcytotic pathways for IgG transport by FcRn are distinct and display an inherent polarity, J. Cell Biol. 185 (2009) 673–684.

[57] A. Garg, J.P. Balthasar, Investigation of the influence of FcRn on the distribution of IgG to the brain, AAPS J. 11 (2009) 553–557.

[58] L. D'Hooghe, A. D Chalmers, S. Heywood, P. Whitley, Cell surface dynamics and cellular distribution of endogenous FcRn, PLoS One 12 (2017) 1–16.

[59] L. Xu, M. Xia, J. Guo, X. Sun, H. Li, C. Xu, X. Gu, H. Zhang, J. Yi, Y. Fang, H. Xie, J. Wang, Z. Shen, B. Xue, Y. Sun, T. Meckel, Y.-H. Chen, Z. Hu, Z. Li, C. Xu, H. Gong, W. Liu, Impairment on the lateral mobility induced by structural changes underlies the functional deficiency of the lupus-associated polymorphism FcγRIIB-T232, J. Exp. Med. 213 (2016) 2707–2727.

[60] W. Hu, Y. Zhang, X. Sun, T. Zhang, L. Xu, H. Xie, Z. Li, W. Liu, J. Lou, W. Chen, FcγRIIB-I232T polymorphic change allosterically suppresses ligand binding, eLife 8 (2019) e46689.

[61] P.G. Saffman, M. Delbrück, Brownian motion in biological membranes, Proc. Natl. Acad. Sci. 72 (1975) 3111–3113.

[62] Y. Gambin, R. Lopez-Esparza, M. Reffay, E. Sierecki, N.S. Gov, M. Genest, R. S. Hodges, W. Urbach, Lateral mobility of proteins in liquid membranes revisited, Proc. Natl. Acad. Sci. 103 (2006) 2098–2102.

[63] F. Höfling, T. Franosch, Anomalous transport in the crowded world of biological cells, Rep. Prog. Phys. 76 (2013).

[64] A. Kusumi, Y. Sako, M. Yamamoto, Confined lateral diffusion of membrane receptors as studied by single particle tracking (nanovid microscopy). Effects of calcium-induced differentiation in cultured epithelial cells, Biophys. J. 65 (1993) 2021–2040.

[65] P. Bruhns, B. Iannascoli, P. England, D.A. Mancardi, N. Fernandez, S. Jorieux, M. Daëron, Specificity and affinity of human Fcγ receptors and their polymorphic variants for human IgG subclasses, Blood 113 (2009) 3716–3725.

[66] F. Spiegel, M.F.W. Trollmann, S. Kara, M. Pöhnl, A.F. Brandner, F. Nimmerjahn, A. Lux, R.A. Böckmann, Role of lipid nanodomains for inhibitory FcγRIIb function, bioRxiv (2023).